

Direct measurement of electron numbers created at infrared laser-induced ionization of various gases

A. Sharma¹, M. Slipchenko¹, K. A. Rahman¹, M. N. Shneider² and A. Shashurin¹

¹Purdue University, West Lafayette, IN, USA

²Princeton University, Princeton, NJ, USA

Abstract

In this work we present temporally resolved measurements of electron numbers in infrared laser-induced plasmas. The experiments were conducted in O₂, Xe, Ar, N₂, Kr and CO at room temperature and atmospheric pressure by a 800 nm femtosecond laser pulse. Rayleigh Microwave Scattering (RMS) technique was used to directly measure the electron numbers using homodyne detection system. Plasma decay after the laser pulse was governed by two competing processes, creation of new electrons by ionization of the metastable atoms and loss of the electrons due to dissociative recombination.

Introduction

Broad research history of the laser-induced plasmas is related to studies of various nonlinear effects at laser beam propagation such as laser pulse filamentation, laser beam collapse, self-trapping, dispersion, modulation instability, pulse splitting etc. [1,2,3,4,5]. These effects are various manifestations of combined action of focusing Kerr nonlinearity (optical Kerr effect) and defocusing nonlinearity due to plasmas. Nowadays laser-induced plasmas find very wide application for plasma-assisted combustion, combustion diagnostics, laser induced breakdown spectroscopy etc [5].

Conventional techniques for diagnostics of atmospheric plasma pose detrimental limitations, the sensitivity of laser interferometry is limited to $n_e \geq 10^{16}$ - 10^{17} cm⁻³ due to the minimal measurable shifts of the interference fringes [6,7,8]. Number of semi-empirical methods for relative measurements of plasma density were proposed as well; however, all of them require absolute calibration based upon theoretically predicted values of plasma number density. Time-of-flight (TOF) mass spectrometer measurements of ion currents generated by laser-induced plasma have been conducted to measure photoionization rates [1,9,10]. The measurement relied on theoretical estimation of total number of electrons in focal zone in order to conduct absolute calibration of the system. Very recently, scattering of THz radiation from the laser-induced plasmas was proposed for spatially unresolved relative measurements of n_e [10,11]. Other measurement techniques were proposed recently based on measurements of capacitive response times of system including capacitor coupled with laser-induced plasma loaded inside [11,12,13]. These attempts to measure n_e in laser-induced plasmas are characterized by various degrees of success and reliability of obtained data, but none of them provides ultimate solution for absolute plasma density measurements until today.

RMS technique enables measurement of total number of electrons (N_e) in the laser-induced plasma [14,15,16]. Very recently, electron numbers generated at femtosecond-laser ionization of air at atmospheric pressure was measured [15]. However, direct measurements of N_e for variety of other important gases were not conducted before. This work is intended

to fill this gap by conducting measurements of number of electrons generated by femtosecond laser pulse in O₂, Xe, Ar, N₂, Kr and CO.

Experimental Details

Schematic of the experimental setup is shown in Fig. 1. Ti:Sapphire laser was used to produce laser pulses at 800nm having FWHM 134 fs, which were focused into a positive pressure chamber using plano-convex lens of 1m focal length. The laser was operated at 100 Hz repetition rate. Diameter of the beam incident on the lens was 7 mm. A quarter wave plate and thin film polarizer were used to control the intensity of the beam, which was measured using a laser power meter (Gentec-EO XLP12-3S-H2-DO) placed after the lens. The positive pressure chamber was made in-house. Thin polythene film was used for the walls of the chamber. It had small apertures for entry and exit of the laser beam and in order to maintain continuous flow of the gas. The duration of the pulse was measured using single shot autocorrelation (Light Conversion TiPA) and was logged throughout the experiment to ensure no drift in laser characteristics was taking place. For this work $w_o=93.6 \mu\text{m}$, $z_R=26.9 \text{ mm}$ [16,17].

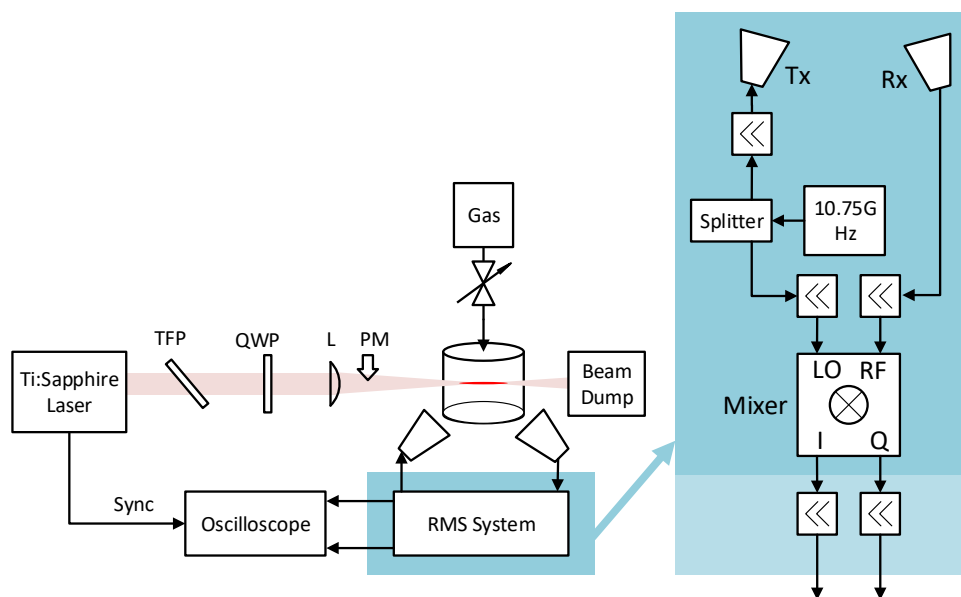


Fig. 1. Femtosecond laser experimental setup and RMS homodyne measurement system. Laser operates at 800 nm wavelength with 100 Hz repetition frequency. The beam passes through thin film polarizer (TFP), quarter wave plate (QWP) which are used to control laser power measured using power meter (PM). The beam is focused using 1000 mm plano-convex (L) lens. The RMS system is calibrated using dielectric Teflon scatterers of know dimensions. For the dielectric scatterers, the output signal right after mixer without additional amplification (32 dB power) is recorded. Teste gases used: O₂, Xe, Ar, N₂, Kr and CO¹⁷.

RMS technique was used to measure the total number of electrons in the laser-induced plasma. Microwave radiation was used to irradiate the plasma. The polarization of the microwave electric field was kept along the direction of the elongated plasma volume. The plasma volume was located far enough from the microwave horn so that incident electric field was uniform across width of the plasma [16,17]. The plasma volume was polarized under the influence of the microwave field and radiated as dipole antenna. Since the amplitude of radiation was uniform everywhere inside the plasma channel, the scattered radiation in the far field is analogues to that of the Hertzian dipole. This process is equivalent

to elastic scattering of light in the Rayleigh regime when wavelength of the light is much greater than the size of the scatterer. The scattered signal from the plasma is proportional to number of electrons inside the scattering volume. The RMS system was calibrated using dielectric of known properties as scattering medium which enables absolute determination of electron numbers. Eq. (1) is the governing equation used for measuring the total number of electrons in the plasma. Where, N_e - total number of electrons, e - electron charge, m_e - electron mass, ν - electron-gas collision frequency, V - volume of the dielectric scatterer, ω - angular frequency of microwaves, A - system calibration coefficient, ϵ_0 - dielectric permittivity of vacuum, ϵ - dielectric constant of the scatterer material and U_{out} - output signal measured by the RMS system.

$$U_{out} = \begin{cases} A \cdot \frac{e^2}{m_e \nu} \cdot N_e & \text{for plasma} \\ A \cdot V \cdot \epsilon_0 (\epsilon - 1) \omega & \text{for dielectric scatterer} \end{cases} \quad (1)$$

For this experiment, homodyne detection-based RMS system was used. Microwave source having frequency 10.75 GHz was used to irradiate the plasma volume. The output of the source was divided in to two branches using a splitter. One branch carried the microwaves to the radiating horn after amplification. The other branch was connected to the LO port of the I/Q mixer. The scattered signal was received by a second horn, amplified and carried to the RF port of the mixer. The output of the mixer was again amplified and connected to oscilloscope to record the data.

The calibration of the RMS system was done by using Teflon dielectric bullets having cylindrical shape with length 10 mm, diameter 3.175 mm and relative permittivity 2.1. The bullet was propelled using a pneumatic gun through the microwave field. The path of dielectric scatterers was chosen to be same as the path of the laser beam in the later experiments. Fig. 2 shows the output signal of the RMS system produced by Teflon bullet. The system calibration coefficient was found to be $A = 6.72 \cdot 10^5 \text{ V}\Omega \text{ m}^{-2}$.

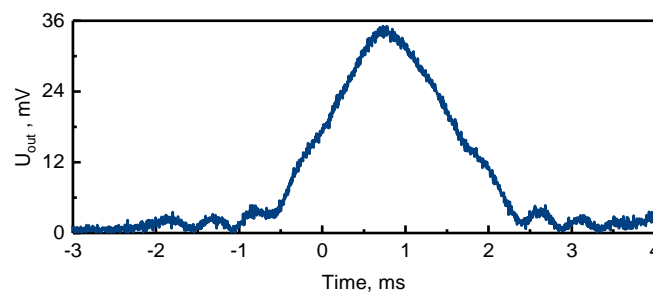


Fig. 2. Temporal evolution of microwave signal scattered due to Teflon bullet used for calibration of RMS system

Experimental setup shown in Fig. 3 was used to study contribution of the non-linear processes in laser beam propagation [5]. The system used the same 1000 mm lens as used in the setup shown in Fig. 1. The diverging beam after the focus was reflected from a pair of beam sampler onto a beam profiler. Each reflection reduced the intensity of the beam by 5%. Beam diameter was measured by Newport LBP2-VIS2 Laser Beam Profiler. Measurements of the beam diameter were made for different pulse energies at two location after the focus. The details of the measurements and analysis of the results are presented below.

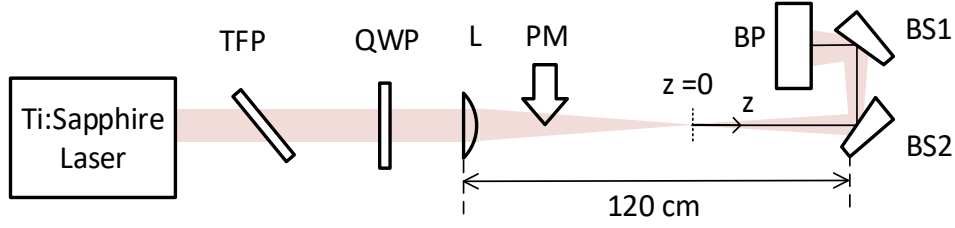


Fig. 3. The Nonlinearity due to Kerr effect was examined by taking beam profiler measurements using beam profiler (BP) located at distance $z_1=67\text{cm}$ and $z_2=80\text{cm}$. for different beam intensities. A pair of wedge beam samplers (BS) were used to reduce the intensity of the beam after focus to prevent saturation of BP.

Results and Discussion

The moment of inception of non-linear effects was determined using the setup shown in Fig. 3. To this end, the beam radius w was measured in ambient air at two locations after the focus, namely $z_1=67\text{ cm}$ and $z_2=80\text{ cm}$, for different laser pulse energies. Fig. 4 shows dependence of beam radius vs. laser pulse energy and demonstrates three characteristic images of the beam profiles taken for $E=80, 320$ and $640\text{ }\mu\text{J}$. Ideal Gaussian beam optic values of the beam radius are also shown as horizontal lines. One can see that the beam radius remained constant and approximately equal to the Gaussian beam optic value for laser pulse energies $E_0 < 320\text{ }\mu\text{J}$ and then decreased for higher E_0 . The reduction in beam size is attributed to non-linear Kerr effect near the focal region (Kerr effect dominates over the plasma non-linearity at low end of laser intensities) [5]. Thus, it can be concluded that threshold of non-linear effect inception in air corresponds to the laser pulse energy of $E_0=320\text{ }\mu\text{J}$ and intensity at the beam center at waist $I_0=7.39\cdot 10^{12}\text{ W/cm}^2$.

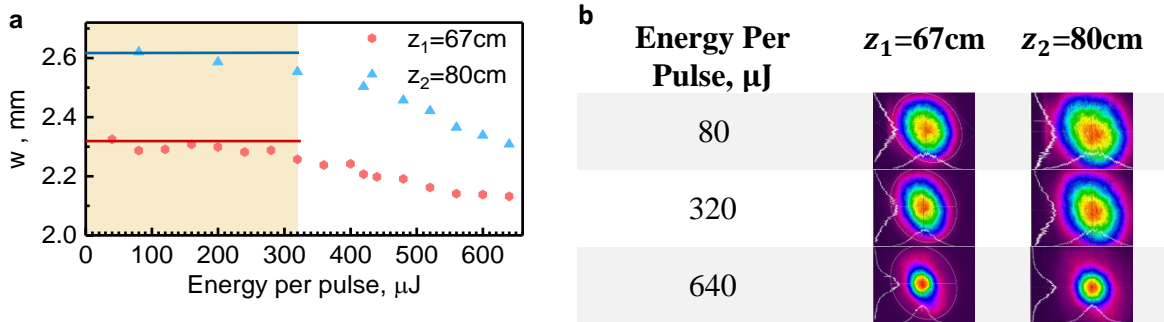


Fig. 4. Measurements of Kerr effect inception threshold in air. **a**, Dependence of the laser beam radius w at two locations after the focus ($z_1=67\text{ cm}$ and $z_2=80\text{ cm}$) vs. laser pulse energy E_0 . **b**, Images of the laser beam profiles for $E_0=80, 320$ and $640\text{ }\mu\text{J}$.

Based on the above findings, photoionization rate and electron number density in O_2 were determined for low laser pulse energies in the range of $220\text{-}320\text{ }\mu\text{J}$. The non-linear effects are negligible in that range of energies and, therefore, the Gaussian beam distribution in vicinity of the focal plane can be used $I(r, z, t) = I_0 \left(\frac{w_0}{w(z)} \right)^2 \exp \left(-\frac{2r^2}{w(z)^2} \right) \exp \left(\left(\frac{t-t^*}{\tau} \right)^2 \right)$, where w_0

is the $1/e^2$ beam radius, $w(z) = \sqrt{1 - \left(\frac{z}{z_R}\right)^2} \cdot w_0$, z_R is the Rayleigh length and τ is the characteristic temporal width of the beam [15,16]. Cross-section of eight-photon ionization of oxygen molecule σ_8 was determined directly from the measurements of spatial and temporal characteristics of the laser beam (τ , w_0 and z_R), measurements of N_e using RMS system for different laser intensities using expression $N_e = \frac{231\pi}{1024 \cdot 16} \sqrt{\frac{\pi}{8}} \sigma_8 n_0 \tau \pi w_0^2 z_R \cdot I_0^8$ following the methodology described in details in Ref. [15]. It was observed that proportionality law $N_e \propto I_0^8$ was satisfied with high accuracy in experiments. Multiphoton ionization rate of O_2 at atmospheric pressure (determined from $\nu = \sigma_8 I_0^8$) and plasma density in the center ($n_{e0} = \frac{N_e}{\frac{231\pi}{1024 \cdot 16} \pi w_0^2 z_R}$) are plotted in Fig. 5.

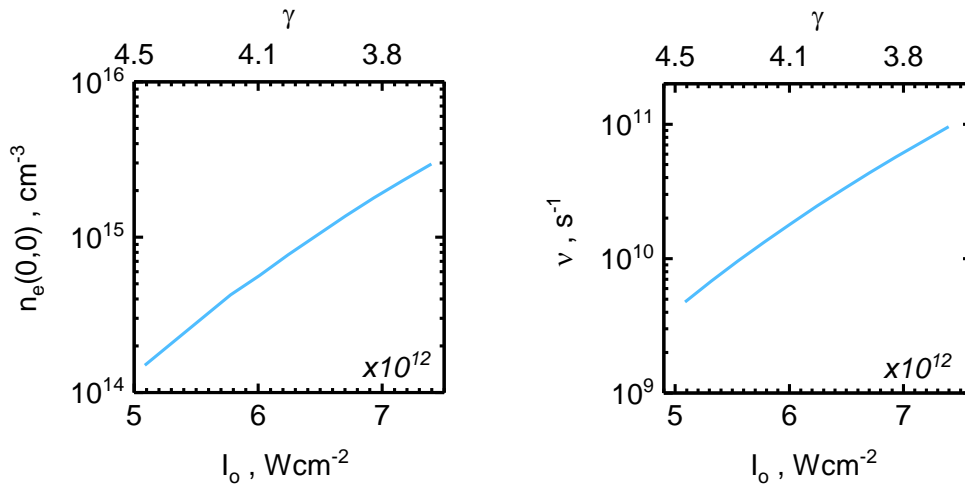


Fig. 5 (a) Multiphoton ionization rate, (b) Plasma density vs. intensity at the centre

Fig. 6 presents log-log plot of the total number of electron in the plasma after laser pulse as a function of laser pulse energy in Xe, O_2 , Kr, CO, N_2 and Ar. Firstly, the total number of electron produced by the laser pulse in all the gases increases as a power function of pulse energy. Xe ionizes the most to produce the highest number of electron from the same pulse energy compared to other gases in the experiment whereas Ar produces the least. The energy requirement for electron generation increases going from left to right. Secondly, the ionization of Xe is ~ 2 orders of magnitude greater than O_2 . Electrons generated in N_2 ($\epsilon_i = 15.6$ eV) and Ar ($\epsilon_i = 15.7$ eV) are almost the same for corresponding pulse energies (450-700 μJ) which is in agreement of their nearly identical ionization potentials. Ionization in Kr is 2 times greater than CO at lower pulse energies (~ 240 μJ) and the difference increases to 10 (~ 370 μJ). Thirdly, at higher pulse energies the electron production starts to saturate. The saturation sets in at ~ 180 μJ in Xe, 370 μJ in Kr, 320 μJ in O_2 and 400 μJ in CO. In N_2 and Ar, there is no onset of saturation for the pulse energies used in the experiments.

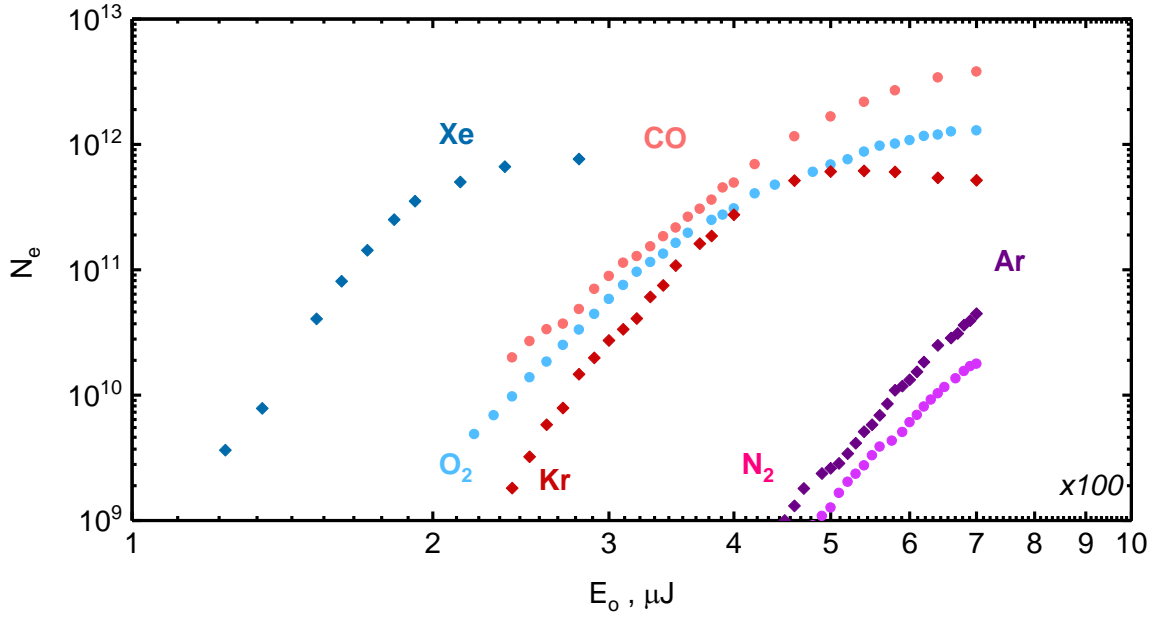


Fig. 6. Total number of electrons generated at photoionization of different gases by 178 fs long, 7 mm diameter laser beam focused using 1000 mm lens.

Temporal decay of electrons is presented in Fig. 7. Electron decay in Ar, Kr, Xe and N₂ can be explained by analysis of two competing processes, namely, creation of new electrons by ionization of the metastable atoms M^* and loss of the electrons due to almost instant conversion of M^+ to M_2^+ and following dissociative recombination.

$$\frac{\partial n_e}{\partial t} = kn_e n_{M^*} - \beta n_e^2 \quad (2)$$

For Ar and Kr, at low laser intensities the metastable density, n_{M^*} is relatively low and the recombination governs the overall decay. At higher laser pulse intensities though, n_{Ar^*} increases and ionization term in the equation is dominant. This causes positive $\frac{\partial n_e}{\partial t}(t=0)$ and corresponding growth of electron density observed in the experiments. Maximum electron density $n_{e,max}$ corresponds to condition $\frac{\partial n_e}{\partial t} = 0$ and can be found as $n_{e,max} = \frac{k}{\beta} n_{M^*}$. Time corresponding to the peak density moment can be estimated as $t_{max} = 1/\beta n_e$. Using $\beta \approx 10^{-7} \text{ cm}^3/\text{s}$ [17] and $t_{max} \sim 10 \text{ ns}$ observed in the experiments plasma density can be estimated as $n_e \sim 10^{15} \text{ cm}^{-3}$. For Xe, coefficient β is significantly larger which results in $\beta n_e > kn_{Xe^*}$ and $\frac{\partial n_e}{\partial t} < 0$, hence the electrons are always decaying, and we don't observe a peak in the electron density evolution. In the case of N₂, the diatomic nature of gas causes the electron-ion recombination to dominate [17]. O₂ and CO have high electron affinity. Eq. (2) can be modified as $\frac{\partial n_e}{\partial t} = -\nu_a n_e - \beta n_e^2$, where attachment to oxygen $\nu_a = k_a \cdot n_M^2$ ($M = \text{O}_2$ and CO) and the reaction constant $k_a \sim 10^{-30} \text{ cm}^6/\text{s}$. [17]. For O₂, $\nu_a = k_a \cdot n_{\text{O}_2}^2 \sim 1.4 \cdot 10^{10} \text{ s}^{-1}$, which gives $\tau_a = \frac{1}{\nu_a} \sim 0.7 \text{ ns}$. The processes involved in the rate equation of electron density, electron attachment and recombination, are always working to reduce the number of electrons in the plasma channel. As result, the extremely fast decay of electron numbers in O₂ and CO can be observed in Fig. 7e and Fig. 7f, where $\tau_{1/2} \sim 0.5 \text{ ns}$ for O₂ and $\sim 1.5 \text{ ns}$ for CO.

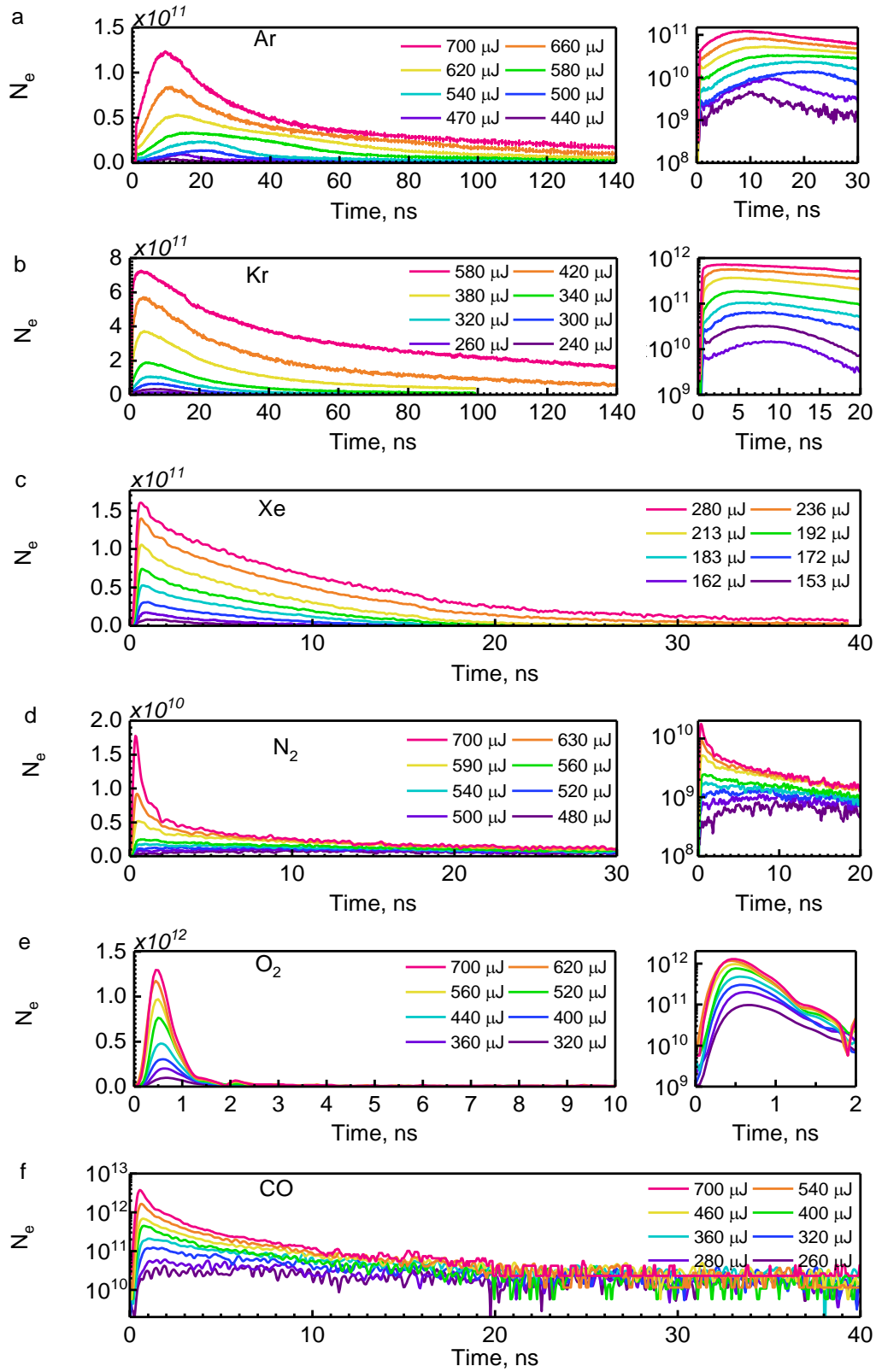


Fig. 7 Temporal evolution of electron numbers in different gases a) Ar, b) Kr, c) Xe, d) N_2 e) O_2 & f) CO

Conclusions

In this work, we have successfully measured the total number of electrons in infrared femtosecond laser pulse for several gases at atmospheric pressure. The method was based on measurement of total electron number in the plasma volume by means of elastic scattering of microwaves off the plasma volume and absolute calibration of the microwave system using dielectric scatterers. We found that Ar and N₂ photoionization rates are close. Ionization rate for Xe and Kr is several orders magnitude greater than that of O₂ and CO, respectively.

References

- [1] Chin, S. L. *Femtosecond Laser Filamentation*, Springer-Verlag, New York, 2010.
- [2] Couairon, A. & Mysyrowicz, A., "Femtosecond filamentation in transparent media," *Phys. Rep.* **441**, 47 (2007).
- [3] Berge, L., Skupin, S., Nuter, R., Kasparian, J. & Wolf, J. P., "Ultrashort filaments of light in weakly ionized, optically transparent media," *Rep. Prog. Phys.* **70**, 1633 (2007).
- [4] Semak, V. V. & Shneider, M. N., "Electromagnetic beam propagation in nonlinear media," *High Power Laser Sci. Eng.* **3**, e11 (2015).
- [5] Semak, V. V. & Shneider, M. N., "Effect of power losses on self-focussing of high intensity laser beam in gases," *J. Phys. D: Appl. Phys.* **46**, 185502 (2013).
- [6] Bodrov, S. *et al.* "Plasma filament investigation by transverse optical interferometry and terahertz scattering," *Optics Express* **19**, 6829 (2011).
- [7] Aleksandrov, N. L. *et al.*, "Decay of femtosecond laser-induced plasma filaments in air, nitrogen, and argon for atmospheric and subatmospheric pressures," *Phys. Rev.* **94**, 013204 (2016).
- [8] Ovsyannikov, A. A. & Zhukov, M. F. *Plasma Diagnostics*, Cambridge International Science Publishing, Cambridge, UK, 2000.
- [9] Talebpour, A., Larochelle, S. & Chin, S. L., "Dissociative ionization of NO in an intense laser field: a route towards enhanced ionization," *J. Phys. B: At. Mol. Opt. Phys.* **30**, 1927 (1997).
- [10] Talebpour, A., Yang, J., Chin, S. L., "Semi-empirical model for the rate of tunnel ionization of N₂ and O₂ molecule in an intense Ti:sapphire laser pulse" *Opt. Comm.* **163**, 29 (1999).
- [11] Ionin, A. A. *et al.*, "Triggering and guiding electric discharge by a train of ultraviolet picosecond pulses combined with a long ultraviolet pulse," *Appl. Phys. Lett.* **100**, 104105 (2012) .
- [12] Mongin, D. *et al.* "Conductivity and discharge guiding properties of mid-IR laser filaments," *Appl. Phys. B*, **122**, 267 (2016).
- [13] Fisher, R. P. *et al.* "Conductivity measurements of femtosecond laser-plasma filaments", *IEEE Trans. Plasma Sci.* **35**, 1430 (2007).
- [14] Shneider, M. N. & Miles, R. B. Microwave diagnostics of small plasma objects. *J. Appl. Phys.* **98**, 033301 (2005).

-
- [15] Sharma, A. *et al.* "Counting the electrons in a multiphoton ionization by elastic scattering of microwaves", *Scientific Reports* **8**, 2874 (2018).
- [16] Sharma, A. *et al.* "Measurements of Electron Numbers in Femtosecond Laser Induced Plasmas Using Rayleigh Microwave Scattering", 2018 AIAA Aerospace Sciences Meeting, AIAA SciTech Forum, (AIAA 2018-0177), <https://doi.org/10.2514/6.2018-0177>
- [17] Raizer, Y. P. *Gas Discharge Physic.* Springer-Verlag Berlin Heidelberg (1991).